Semiconductor Physics, Quantum Electronics & Optoelectronics, 2025. V. 28, No 4. P. 424-431.

Semiconductor physics

Distribution of Mg and Ti atoms over octahedral sites and physical properties of Mg_2TiO_4

N.I. Kashirina[1*], L.V. Borkovska[1], Ya.O. Kashyrina[2], O.S. Muratov[3], O.S. Roik[3]

[1]*V. Lashkaryov Institute of Semiconductor Physics, NAS of Ukraine, 41 Nauky Avenue 03028 Kyiv, Ukraine*
[2]*Frantsevich Institute for Problems of Materials Science, NAS of Ukraine*
3 Omelyan Pritsak Street, 03142 Kyiv, Ukraine
[3]*Taras Shevchenko National University of Kyiv, Faculty of Chemistry,*
12 Hetmana Pavla Skoropadskoho Street, 01033 Kyiv, Ukraine
[*]*Corresponding author e-mail: kashirina1506@gmail.com*

Abstract. Ceramics based on Mg_2TiO_4 (MTO) are widely used in numerous modern quantum electronic devices. The present paper deals with a study of cubic and tetragonal modifications of MTO. The band gap and electron state density of the cubic MTO are calculated for different distributions of Mg and Ti atoms over octahedral positions in the unit cell. Both random distributions of atoms over the octahedral positions and highly symmetric combinations are considered. The band gap as a function of the total energy of the unit cell is constructed. The band gap width increases at decreasing the free energy of a crystal. The highly symmetric distribution of atoms over the octahedral positions is shown to lead to a transition from cubic MTO to tetragonal syngony with a lower energy compared to an MTO cubic crystal with a random distribution of atoms over the octahedral positions. The band gap width for the cubic Mg_2TiO_4 with a random distribution of Mg and Ti atoms over the octahedral positions calculated by us using Vienna Ab initio Simulation Package (VASP) was 4.086 eV. The obtained results are in a good agreement with experimental data. The calculated band gap width for tetragonal MTO was 4.988 eV.

Keywords: Mg_2TiO_4, inverse spinel, VASP, band structure calculation, density of states.

https://doi.org/10.15407/spqeo28.04.424
PACS 61.66.-f, 77.84.Cg

Manuscript received 09.08.25; revised version received 07.10.25; accepted for publication 26.11.25; published online 15.12.25.

1. Introduction

Ceramics based on Mg_2TiO_4 (MTO) are widely used for producing refractory materials [1, 2], electrodes in magnesium ion batteries [3, 4] as well as in high-precision quantum electronics devices for fabricating resonators, filters, and antennas operating at microwave frequencies [5–9]. Recently, significant progress has been achieved in production of compact and stable white-light light-emitting diodes (LEDs) with excellent performance characteristics and a long service life [10]. MTO with Mn^{4+} impurities is a promising material for fabricating such LEDs due to its relative cheapness and good prospects for achieving desired optical characteristics of light emission by substitution of Ti^{4+} ions with Mn^{4+} ions [11, 12].

In cubic MTO, 8 Ti atoms and 8 Mg atoms are randomly located in octahedral positions. This circumstance complicates calculation of the band structure of the cubic MTO because one or another specific arrangement of atoms in the unit cell must be selected. The same applies to the calculations of the energy of a crystal with impurity atoms [13]. Experimental values of the zone width vary from 3.55 eV [14] to 4.33 eV [12]. The band gap values of MTO nanoparticles range between 3.26 and 3.78 eV [15]. Note that the experimental value of the cubic MTO band gap of 4.33 eV [12] is close to the value of 4.4 eV obtained for $MgTiO_3$ crystals [16].

The value of the band gap of 2.4 eV was obtained theoretically [13] using Vienna Ab-initio Simulation Package (VASP) [17] with the Perdew–Wang functional (PW91) [18] within the generalized gradient approximation (GGA). It should be noted that this value is significantly lower than the respective experimental results.

In this work, we studied the effect of a choice of the distribution of Mg and Ti atoms over octahedral positions on the energy of the crystal lattice and the band gap. Both random distributions of atoms over the octahedral positions and highly symmetrical combinations were considered. At this, one of the structures studied here was the one considered in [13].

2. Crystal structure of Mg_2TiO_4

Magnesium orthotitanate forms colorless crystals of tetragonal syngony belonging to the space group $P4_122$. The unit cell parameters are a_t = 5.9748 Å, c_t = 8.414 Å, and Z = 4. At temperatures above 700 °C, transition to cubic syngony phase occurs. This syngony belongs to the space group $Fd3m$, and the unit cell parameters are a_c = 8.4376 Å, and Z = 8 [19]. The method for obtaining MTO is described in [12]. Note that the unit cell parameters of the cubic MTO may slightly differ in different sources [11, 12, 19–21]. Thus, in [11], the unit cell parameter of the cubic MTO is a_c = 8.4452 Å, while the diffraction pattern obtained in [12] corresponds with high accuracy to the results provided in [21], where the unit cell parameter is a_c = 8.4409 Å. For the calculations performed in the present work, we choose this structure as the initial one. The initial CIF file used in our calculations was taken from the database [22]. The MTO unit cell is described in [21]. Fig. 1 shows the MTO structure typical for cubic crystals with inverse spinel structure, constructed using VESTA software [23]. Magnesium atoms occupy tetrahedral positions as well as octahedral positions, which they share with titanium atoms randomly distributed among them. Hence, the occupancy of the latter position by both Mg and Ti atoms is 0.5. Then, 8 magnesium atoms and 8 titanium atoms can occupy any of the 16 octahedral positions of the MTO with equal probability. The unit cell of the MTO consists of 56 atoms and is shown in Fig. 1. Fig. 2 shows an example of a structure with one of the possible distributions found using a random number generator (8 positions out of 16 possible ones).

To calculate the crystal characteristics, one should select the positions of the atoms included in the unit cell. In this case, both the energy of the crystal and its physical characteristics such as the band gap, the density of states (DOS) and the band structure will depend on the distribution of atoms in the unit cell. The subset of Mg and Ti atoms occupying the octahedral positions in the unit cell, the coordinates of which are given in Table 1, corresponds to a distribution similar to that in an amorphous state.

2. Algorithm for calculating various atom distributions over octahedral positions

The structure of the unit cell of MTO consisting of 56 atoms, the 16 of which fill the octahedral positions (8 Ti atoms and 8 Mg atoms) with equal probabilities, is shown in Fig. 1. We fill these positions according to certain rules, which are as follows:

1. Let us number the coordinates of the 16 octahedral positions in the MTO lattice. In Table 1, this numbering is presented in the column “Position”. Next, we should go through all the possible arrangements of r = 8 Ti atoms in n = 16 positions, excluding identical combinations that appear as a result of taking into account the positions associated with permutation of identical atoms, *i.e.*, taking into account the indistinguishability of the atoms of one element among themselves. The number of such arrangements of the atoms in the unit cell can be calculated using the following expression:

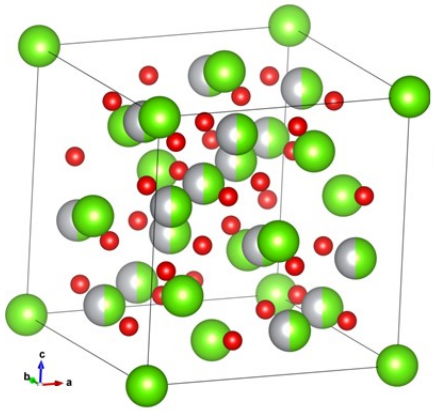

Fig. 1. Unit cell of Mg_2TiO_4. Magnesium (green) and titanium (gray) atoms are distributed over octahedral positions (gray-green) with equal probabilities, oxygen corresponds to red spheres.

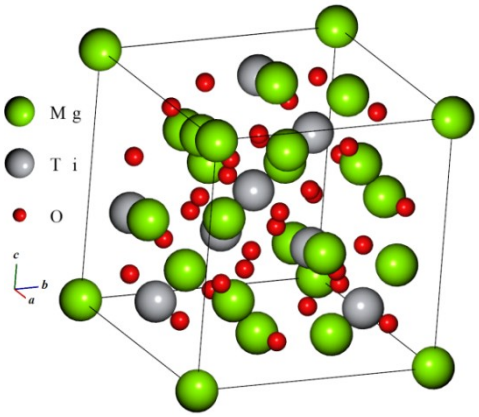

Fig. 2. Unit cell of Mg_2TiO_4. Magnesium and titanium atoms are randomly distributed over octahedral positions (one of the possible combinations is shown).

$$N = \frac{A_n^r}{r!} = C_n^r = \frac{n!}{(n-r)!r!},\ C_{16}^8 = 12870. \qquad (1)$$

This procedure may be characterized as generating combinations of 8 list elements by 16 positions without repetitions. The algorithm used to find all the possible configurations is included in the standard library of Python 3 language [24]. An example of the used algorithm is presented on the website [25].

2. It is logical to assume that some structures are spatially equivalent to others, so we reduced the number of the studied combinations as follows:

a. Using an atomic simulation environment (ASE) package [26] and a Spglib module [27], the space group of each unit cell was determined.

b. The entire set of the structures was divided into subgroups depending on the found space symmetry group. Using the algorithm presented in [28], the equivalence of any two structures within each subgroup was determined. If any such structures were found, the second structure was removed from subsequent comparison. The process continued until the structures in the group were exhausted.

Table 1. Coordinates of 16 octahedral positions where Mg and Ti atoms can be located.

Position	X	Y	Z	Position	X	Y	Z
1	0.375	0.375	0.375	9	0.875	0.125	0.625
2	0.375	0.875	0.875	10	0.875	0.625	0.125
3	0.875	0.375	0.875	11	0.375	0.125	0.125
4	0.875	0.875	0.375	12	0.375	0.625	0.625
5	0.125	0.875	0.625	13	0.125	0.625	0.875
6	0.125	0.375	0.125	14	0.125	0.125	0.375
7	0.625	0.875	0.125	15	0.625	0.625	0.375
8	0.625	0.375	0.625	16	0.625	0.125	0.875

3. Several configurations that modeled statistical distribution of the atoms over the octahedral positions (such combinations, as a rule, corresponded to MTO unit cells with no symmetry elements) were randomly selected from the obtained structures. Moreover, at least one structure representing each specific space group was selected.

3. Energy and band gap of MTO

Table 2 presents the total energy of the crystal cell and the corresponding band gaps for different distributions of Mg and Ti atoms over the octahedral sites. The calculations were performed using the Heyd–Scuseria–Ernzerhof (HSE) hybrid functional [29]. The values marked with asterisks were calculated using Quantum Espresso (QE) program [30] with the Gaussian–Perdue–Burke–Ernzerhof (GAUPBE) hybrid functional [31]. In the column "Positions occupied by Ti", various arrangements of 8 Ti atoms in 16 octahedral positions are presented. The remaining octahedral positions are occupied by Mg atoms. The coordinates of the atoms in the octahedral positions are numbered according to Table 1.

The numbering of the various structural configurations is presented in the column "Structure". The distribution of atoms No 1 in the column "Structure" corresponds to the MTO unit cell considered in [13]. Five subgroups were randomly selected from the obtained structural subgroups (they are designated by ordinal numbers 2–6 in the "Structure" column in Table 2). Moreover, one example corresponding to other possible spatial groups was also given. In total, 23 combinations are presented in Table 2. The combination No 23 corresponding to the space group $P4_122$ illustrates the possibility of structural transition from cubic to tetragonal symmetry with structural ordering of atoms over the octahedral sites of the MTO unit cell. This space symmetry group corresponds to the tetragonal modification of MTO, which contains not 56, but 28 atoms in the unit cell. The structure No 24 corresponds to the MTO tetragonal syngony. The energy is halved (in absolute value) compared to the same structure No 23 due to the fact that the number of atoms in the unit cell is half as much. The tetragonal modification of MTO has a lower energy per atom compared to the cubic modification with a statistical distribution of Ti and Mg atoms over the octahedral positions, *i.e.* it is more stable. Structural transition from the tetragonal to the cubic syngony of the MTO occurs at a temperature above 700 °C [19]. This transition can be explained by the fact that with an increase in temperature, the highly symmetric distribution of atoms over octahedral positions changes to a statistical distribution, *i.e.* the crystal sublattice corresponding to the octahedral positions "melts" and transforms into a disordered state. When the crystal is rapidly cooled, the high-temperature cubic modification of the MTO retains its properties. At low temperatures, the cubic modification of MTO exists as a metastable state, separated from the stable state corresponding to the tetragonal modification of Mg_2TiO_4 by a potential barrier. Phase transition between the cubic and tetragonal structures occurs with conservation of the molar volume [19]. The features of the temperature transitions from the cubic to tetragonal syngony and the reverse transition for epitaxial MTO films were studied in [32]. In [33] the transition from the cubic to the tetrahedral modification of MTO under pressure was investigated. In all cases, the phase transition to the tetragonal structure occurs as a result of ordering of Mg and Ti atoms over the octahedral positions. Natural modification of Mg_2TiO_4 corresponds to the tetragonal structure, which is a slightly distorted cubic one [19, 32].

The total energy and band gap of MTO with different arrangements of Mg and Ti atoms in octahedral sites are presented in Table 2. The energy and band structure of the MTO were calculated by the ab initio

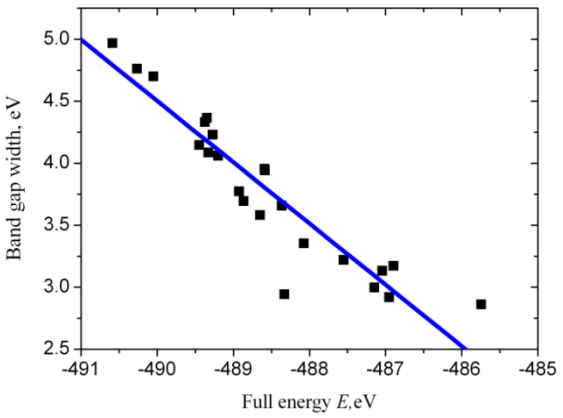

Fig. 3. Dependence of the band gap width of Mg_2TiO_4 on the unit cell energy.

Table 2. Total energy and band gap width for different arrangements of Ti and Mg atoms in octahedral positions of Mg_2TiO_4.

Structure No	Positions occupied by Ti	Space symmetry group of the model unit cell	Total energy, eV (HSE, VASP)	ΔE, eV (HSE, VASP)
1	1, 4, 5, 7, 9, 10, 13, 16 [13]	C 2/m	–489.1974565	4.06, 4.3*
2	1, 2, 3, 5, 6, 7, 8, 16	P 1	–488.9228768	3.774, 3.78*
3	3, 4, 5, 8, 13, 14, 15, 16	C 2/m	–489.3718661	4.331
4	1, 3, 4, 8, 9, 10, 15, 16	P 1	–487.0414256	3.132
5	1, 4, 6, 7, 9, 10, 11, 15	P 1	–487.549394	3.221
6	1, 5, 7, 8, 11, 13, 14, 15	P 1	–489.3258126	4.086, 4.01*
7	1, 2, 5, 8, 11, 12, 14, 15	P 2	–486.9532775	2.918
8	1, 2, 3, 6, 8, 11, 12, 14	C m	–487.1469256	2.997
9	2, 3, 8, 10, 13, 14, 15, 16	C 2	–488.6478972	3.581
10	1, 2, 3, 4, 11, 12, 13, 15	P –1	–488.8634797	3.694
11	1, 3, 4, 6, 7, 8, 10, 15	C m m 2	–486.8945498	3.171
12	3, 4, 5, 7, 9, 11, 15, 16	P 4_1	–488.5856688	3.943
13	1, 3, 4, 7, 9, 11, 12, 13	C 2 2 2_1	–490.2643026	4.761
14	2, 3, 6, 8, 10, 11, 13, 15	P –4	–488.3620478	3.658
15	4, 5, 7, 8, 10, 11, 12, 13	P 2_1	–489.2704516	4.229
16	2, 4, 7, 8, 11, 12, 13, 15	P 4_3	–488.5901718	3.954
17	1, 2, 5, 6, 11, 12, 13, 14	P –4 m 2	–485.7435037	2.86
18	5, 6, 7, 8, 9, 11, 14, 16	P 2_1/m	–488.0746084	3.355
19	1, 4, 6, 7, 9, 12, 14, 15	P m a 2	–488.3289842	2.942
20	1, 4, 9, 10, 11, 12, 13, 16	P 2/c	–490.0479063	4.7
21	1, 2, 3, 4, 5, 6, 7, 8	I m m a	–489.4465001	4.146
22	1, 4, 5, 8, 10, 11, 13, 16	P 4_3 2 2	–490.588277	4.967
23 (Tetr.)	2, 3, 5, 8, 10, 11, 14, 15	P 4_1 2 2	–490.588282	4.967
24 (Tetr.)		P 4_1 2 2	–256.9955726	4.988

Note: *calculations performed in Quantum Espresso (QE) program [30] using the Gaussian–Perdue–Burke–Ernzerhof (GAUPBE) hybrid functional [31].

method within the framework of the density functional theory using a VASP software package [17], developed for calculating and modeling electronic structure and molecular dynamics of crystal lattices of solids and liquids. For Mg, Ti, and O atoms, the PAW pseudo-potentials were chosen for the valence electrons filling the $3s^2$ (PAW_GGA Mg 05Jan2001), $3d^24s^2$ (PAW_GGA Ti 08Aug2001) and $2s^22p^4$ (PAW_GGA O_s 04May1998) shells, respectively. The cutoff energy was assumed to be 520 eV. The unit cell of pure MTO contains 8 Ti, 16 Mg, and 32 O atoms. The unit cell parameter of the initial cubic MTO was taken to be 8.440 Å. The Brillouin zone for the 56-atom unit cell was calculated using a 3×3×3 *k*-point grid. The energy convergence was at least 10^{-5} eV/atom. Fig. 3 shows the dependence of the band gap on the unit cell energy for different spatial distributions of Mg and Ti atoms over the octahedral positions. With a decrease in the unit cell energy (increase in its absolute value), the band gap increases. The random distribution of atoms over the positions in the MTO unit cell shown in Fig. 2 corresponds to the structure No 6 in Table 2.

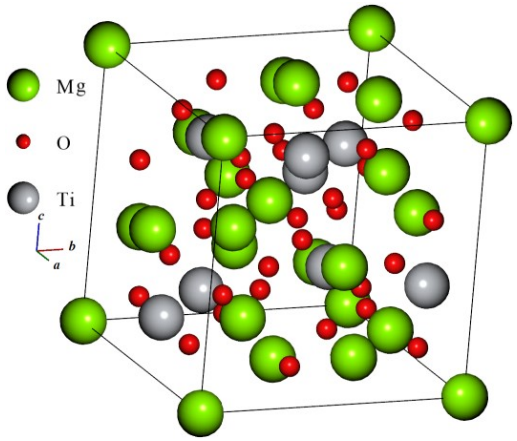

Fig. 4. Crystal structure of tetragonal MTO (56 atoms in a unit cell, the structure No 23 in Table 2).

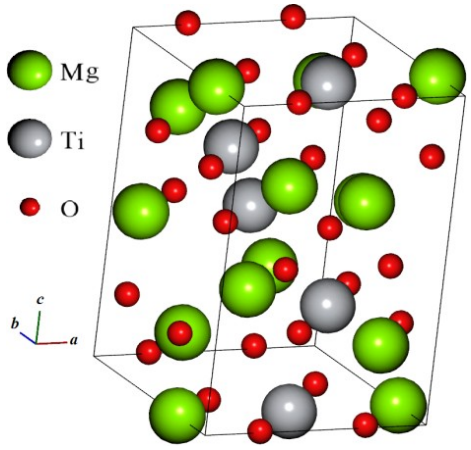

Fig. 5. Crystal structure of tetragonal MTO (28 atoms in a unit cell, the structure No 24 in Table 2).

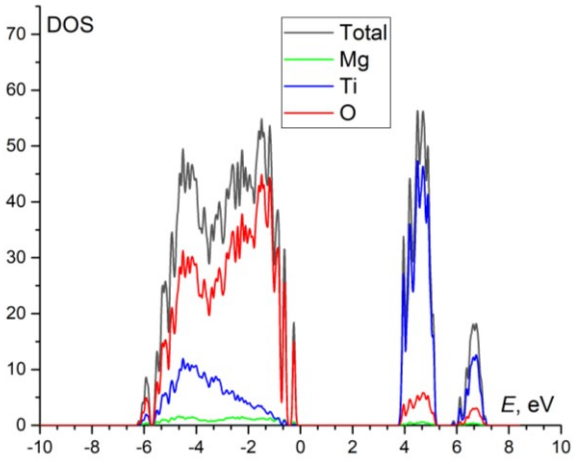

Fig. 6. Density of states for the cubic MTO, the configuration No 6 in Table 2 (56 atoms in a unit cell). Unit cell parameters and volume are $a_c = 8.4398$ Å and $V_c = 601.176$ Å^3.

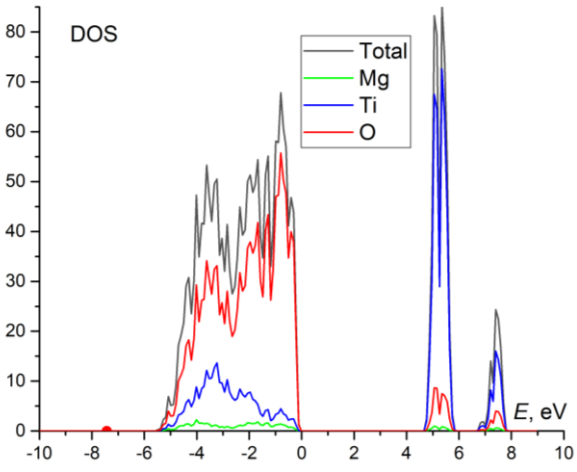

Fig. 7. Density of states for the tetragonal MTO, the configuration No 23 in Table 2 (56 atoms in a unit cell). Crystal cell parameters and volume are $a_{ct} = 8.4505$, $c_{ct} = 8.4198$, and $V_{ct} = 601.266$.

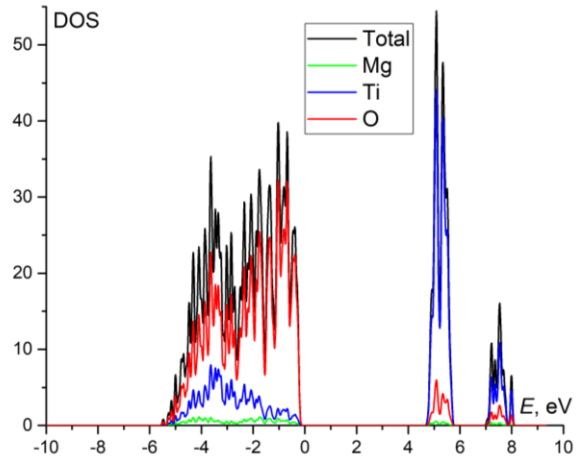

Fig. 8. Density of states for the tetragonal MTO, the configuration No 24 in Table 2 (28 atoms in a unit cell). The unit cell parameters are $a_t = 5.9758$ Å, $c_t = 8.3948$ Å, and $V_t = 299.78$ Å^3.

Fig. 4 shows an MTO structure with a highly symmetric distribution of atoms over the octahedral positions, corresponding to the structure No 23 in Table 2. This structure is equivalent to the MTO of the tetragonal syngony with a unit cell consisting of 28 atoms (structure No 24) shown in Fig. 5. Possible orientations of a unit cell consisting of 28 elements relative to a cubic structure are analyzed in [32].

The values of the band gap presented in Table 2, marked with asterisks, were calculated using a QE software package [30] with the Gaussian-Perdue–Burke–Ernzerhof (GAUPBE) hybrid functional [31].

Figs. 6, 7, and 8 show the densities of states for various MTO configurations. Fig. 6 uses the configuration corresponding to the space group P1 as an example (random distribution of Mg and Ti atoms over the octahedral positions, no symmetry elements, this is the configuration No 6 in Table 2). Fig. 7 shows an example of the DOS for a configuration with an ordered arrangement of Mg and Ti atoms over the octahedral positions (configuration No 23, space group P 4_1 2 2). Fig. 8 shows the DOS for the tetragonal MTO structure obtained by VASP calculation for a unit cell consisting of 28 atoms, the configuration No 24 in Table 2.

4. Conclusions

The paper considers various options for ordering Ti and Mg atoms over octahedral positions of a cubic MTO crystal. It is shown that calculations of the crystal lattice energy and band structure parameters performed with VASP and QE software packages lead to satisfactory agreement between the results obtained using the Heyd–Scuseria–Ernzerhof (HSE) [36] functional and the GAUPBE (QE) hybrid functional.

The band gap increases with decrease in the unit cell energy and depends on the distribution of atoms over the octahedral positions. The lowest energy state of the crystal lattice corresponds to an MTO crystal with

tetragonal symmetry. At increasing temperature, the MTO crystals with the tetragonal symmetry transform into the cubic MTO due to disordering of Ti and Mg atoms over the octahedral positions.

Phase transitions associated with ordering of atoms in the octahedral positions characterized by appearance of a short-range order in normal spinels with the space group Fd–3m and inverse spinels $P4_122$ were studied in [34] using the Monte Carlo method. The calculations were carried out in the temperature range from 0 to 3000 K with a step of 100 K. The materials $MgAlGaO_4$, $MgAl_2O_4$, $MgGa_2O_4$ were considered as samples. Unlike Ref. [34], we investigated not the transitions between the reverse and direct spinels, but ordering of the Ti and Mg cations over the octahedral positions in the reverse spinel. The tetragonal structure of the MTO can be characterized as a type of reverse spinel with a high degree of ordering of the Mg and Ti cations over the octahedral positions.

The calculated crystal cell parameters of the tetragonal MTO with a crystal cell consisting of 56 atoms (No 23 in Table 2) are a_{ct} = 8.4505 Å, c_{ct} = 8.4198 Å, and V_{ct} = 601.266 Å^3. This structure is a slightly distorted cubic cell of MTO with the calculated cell parameters a_c = 8.4398 Å and V_c = 601.176 Å^3 (No 6 in Table 2). The tetragonal crystal cell of MTO consisting of 56 atoms corresponds to a slight compression along ***c*** and extension along ***a*** of the cubic cell. Phase transition from the cubic to the tetragonal structure occurs without changing the molar volume of the crystal V_c [19]. The crystal cell corresponding to the tetragonal structure shown in Fig. 4 is not the unit cell of MTO. Due to the ordering of Mg and Ti atoms over the octahedral positions, the unit cell of the tetragonal MTO contains not 56, but 28 atoms. Recalculation of the crystal cell parameters a_{ct} and c_{ct} shown in Fig. 4, into the parameters a_t and c_t of the unit cell consisting of 28 atoms shown in Fig. 5 can be carried out according to the rule $a_t = a_{ct}/\sqrt{2}$ = 5.9754 and $c_t = c_{ct}$ = 8.4198 Å. The calculated values of the unit cell parameters for the 28-atom cell are a_t = 5.9758, c_t = 8.3948 Å, and V_t = 299.78 Å^3. The experimental values of the cubic and tetragonal unit cell parameters of MTO obtained in [19] are a_c = 8.4376 Å, V_c = 600.71 Å^3 and a_t = 5.9448 Å, c_t = 8.414 Å, V_t = 300.77 Å^3. Note that calculation with the crystal cell parameters of the tetragonal modification of MTO, performed with 56 atoms, gives better agreement with the experiment than the calculation performed for the unit cell with 28 atoms.

In [13, 35], the band structure of the cubic modification of MTO was calculated using the GGA functional [18]. The model of the cubic MTO crystal lattice used for the calculations in [35] corresponds to the configuration No 1 in Table 2. The band gap calculated in [35] was 2.2 eV, which is significantly lower than the experimental values lying in the range of 3.7 to 4.42 eV (see [35] and the references therein). Use of the HSE functional significantly improved the agreement with the experiment for the band gap value of the MTO.

Therefore, the band gap for the cubic MTO lattice model proposed in [36], calculated by us, was 4.06 eV. The band gap of 4.331 eV corresponding to the structure No 3 in Table 2 reproduces with high accuracy the experimental value of 4.33 eV obtained in [12]. At the same time, both the GGA and HSE functionals reproduce with high accuracy the parameters of the crystal structure of both cubic and tetragonal MTO. As a model of the cubic MTO, we selected the structure No 6 in Table 2 having no symmetry elements in the unit cell, since it corresponds to the most numerous structures with random distributions of Ti and Mg atoms over the octahedral positions of the crystal.

References

1. Mandal S., Hemrick J.G., Mahapatra M.K. Chrome-free qandilite (Mg_2TiO_4) refractory aggregates: Role of titania source and evaluation of thermal expansion coefficient. *J. Eur. Ceram. Soc*. 2022. **42**, No 15. P. 7343–7351. https://doi.org/10.1016/j.jeurceramsoc.2022.08.012.
2. Zhao J., Hou Q. Fan B. *et al*. Investigation on mechanical and thermal properties of $MgAl_2O_4$-Mg_2TiO_4 solid solutions with spinel-type structure. *Ceram. Int.* 2023. **49**, No 22. Part A. P. 34490–34499. https://doi.org/10.1016/j.ceramint.2023.08.049.
3. Chakrabarti S., Bisw K. DFT study of Mg_2TiO_4 and Ni doped $Mg_{1.5}Ni_{0.5}TiO_4$ as electrode material for Mg ion battery applications. *J. Mater. Sci*. 2017. **52**. P. 10972–10980. https://doi.org/10.1007/s10853-017-1260-x.
4. Wu X., Dou Y., Lian R. *et al*. Understanding rechargeable magnesium ion batteries via first-principles computations: A comprehensive review. *Energy Storage Mater*. 2022. **48**. P. 344–355. https://doi.org/10.1016/j.ensm.2022.03.039.
5. Chen Y.B. Crystal structure and dielectric properties of $La(Mg_{1-x}Zn_x)_{1/2}Ti_{1/2}O_3$ ceramics at microwave frequencies. *J. Alloys Compd.* 2011. **509**. P. 1050–1053. https://doi.org/10.1016/j.jallcom.2010.09.170.
6. Bhuyan R.K. Ultra-low loss Mg_2TiO_4 based dielectric ceramics for microwave applications: An overview. *Micro and Nanosystems*. 2022. **14**. P. 110–120. https://doi.org/10.2174/1876402912999200825104327.
7. Wang X., Zhou S., Liu K. *et al*. Broad sintering temperature range and stable microwave dielectric properties of Mg_2TiO_4–CeO_2 composite ceramics. *Ceram. Int.* 2022. **48**, No 14. P. 20245–20250. https://doi.org/10.1016/j.ceramint.2022.03.304.
8. Chen Y.B. Sintering temperature dependences of x $[(Mg_{0.6}Zn_{0.4})_{0.95}Co_{0.05}]_2TiO_4$–$(1-x)$ $Ca_{0.8}Sr_2TiO_3$ microwave dielectric ceramics with a zero temperature coefficient of resonant frequency. *J. Ceram. Soc. Jpn.* 2014. **122**(1421). P. 117–121. https://doi.org/10.2109/jcersj2.122.117.
9. Qi H., Yuancheng T., Xiaofeng Z. *et al*. Temperature stable dielectric properties of Mg_2TiO_4–$MgTiO_3$–$CaTiO_3$ ceramics over a wide temperature range.

Ceram. Int. 2022. **49**, No 2. P. 1997–2006. https://doi.org/10.1016/j.ceramint.2022.09.165.
10. Wathook B., Hassan D.A. Modified sol-gel method of synthesising a Mn^{4+}-doped Mg_2TiO_4: A red phosphor for improved LED performance. *Annales de Chimie – Science des Matériaux*. 2024. **48**, No 1. P. 11–16. https://doi.org/10.18280/acsm.480102.
11. Ye J.T., Li S., Wu X. *et al*. Sol–gel preparation of efficient red phosphor Mg_2TiO_4:Mn^{4+} and XAFS investigation on the substitution of Mn^{4+} for Ti^{4+}. *J. Mater. Chem C.* 2013. **1**, No 28. P. 4327–4333. https://doi.org/10.1039/c3tc30553h.
12. Borkovska L.,· Khomenkova L., Markevich I. *et al*. Effect of Li^{+} co-doping on structural and luminescence properties of Mn^{4+} activated magnesium titanate films. *J. Mater. Sci.: Mater. Electron.* 201. 8**29**. P. 15613–15620. https://doi.org/10.1007/s10854-018-9153-6.
13. Huang C.S., Huang C.L., Liu Y.C. *et al*. Ab initio-aided sensitizer design for Mn^{4+}-activated Mg_2TiO_4 as an ultrabright fluoride-free red-emitting phosphor. *Chem. Mater.* 2018. **30**, No 5. P. 1769–1775. https://doi.org/10.1021/acs.chemmater.8b00149.
14. Ristić Z., Dordević V., Medić M. *et al*. Temperature dependence of the Cr^{3+}-doped Mg_2TiO_4 near-infrared emission. *Opt. Mater*. 2021. **120**. P. 111468 (6 p.). https://doi.org/10.1016/j.optmat.2021.111468.
15. Bhuyan R.K., Mohapatra R.K., Nath G. *et al*. Influence of high-energy ball milling on structural, microstructural, and optical properties of Mg_2TiO_4 nanoparticles. *J. Mater. Sci.: Mater. Electron*. 2020. **31**, No 1. P. 628–636. https://doi.org/10.1007/s10854-019-02568-3.
16. Negishi M., Fujiwara K., Tsukazaki A. Formation of ilmenite-type single-crystalline $MgTiO_3$ thin films by pulsed-laser deposition. *AIP Adv*. 2021. **11**, No 12. P. 125125. https://doi.org/10.1063/5.0078021.
17. Kresse G., Furthmüller J. Efficient iterative schemes for ab initio total-energy calculations using a plane-wave basis set. *Phys. Rev. B*. 1996. **54**. P. 11169–11186. https://doi.org/10.1103/PhysRevB.54.11169.
18. Perdew J.P., Burke K., Ernzerhof M. Generalized gradient approximation made simple. *Phys. Rev. Lett.* 1996. **77**, No 18. P. 3865–3868. https://doi.org/10.1103/physrevlett.77.3865.
19. Wechsler B.A., Von Dreele R.B. Structure refinements of Mg_2TiO_4, $MgTiO_3$ and $MgTi_2O_5$ by time-of-flight neutron powder diffraction. *Acta Crystallogr. B*. 1989. **45**. P. 542–549. https://doi.org/10.1107/S010876818900786X.
20. Ropp C.R. Ch. 8 – Group 4 (Ti, Zr and Hf) Alkaline Earth Compounds, in: *Encyclopedia of the Alkaline Earth Compounds,* Elsevier Amsterdam, 2013. P. 653–700. https://doi.org/10.1016/C2012-0-00777-6.
21. McMurdie H., Morris M., Evans E. *et al*. *Standard x-ray diffraction powder patterns ::section 12 – data for 57 substances*. National Institute of Standards and Technology, Gaithersburg, MD, 1975 [online]. https://doi.org/10.6028/NBS.MONO.25-12 (Accessed October 21, 2025).
22. Gražulis S., Daškevič A., Merkys A. *et al*. Crystallography Open Database (COD): an open-access collection of crystal structures and platform for world-wide collaboration. *Nucleic Acids Res.* 2012. **40**, No D1. P. D420–D427. https://doi.org/10.1093/nar/gkr900.
23. Momma K., Izumi F. VESTA 3 for three-dimensional visualization of crystal, volumetric and morphology data. *J. Appl. Crystallogr*. 2011. **44**. P. 1272–1276. https://doi.org/10.1107/S0021889811038970.
24. DOCS Python3. https://docs.python.org/3/
25. Planetcalc. Combinatorics. Combination generator. https://planetcalc.com/3756/#google_vignette
26. Larsen A.H., Mortensen J.J., Blomqvist J. *et al.* The atomic simulation environment – a Python library for working with atoms. *J. Phys.: Condens. Matter*. 2017. **29**, No 27. P. 273002 (9 p.). https://doi.org/10.1088/1361-648X/aa680e.
27. Togo A., Shinohara K., Tanaka I. Spglib: a software library for crystal symmetry search. arXiv:1808.01590 [cond-mat.mtrl-sci] https://arxiv.org/abs/1808.01590.
28. Lonie D.C., Zurek E. Identifying duplicate crystal structures: XtalComp, an open-source solution. *Comput. Phys. Commun.* 2012. **183**. P. 690–697. https://doi.org/10.1016/j.cpc.2011.11.007.
29. Heyd J., Scuseria G.E., Ernzerhof M. Hybrid functionals based on a screened Coulomb potential. *J. Chem. Phys*. 2003. **118**, No 18. P. 8207–8215. https://doi.org/10.1063/1.1564060.
30. Giannozzi P., Andreussi O., Brumme T. *et al.* Advanced capabilities for materials modelling with Quantum ESPRESSO. *J. Phys.: Condens. Matter.* 2017. **29**, No 46. P. 465901 (30 p.). https://doi.org/10.1088/1361-648x/aa8f79.
31. Song J.W., Yamashita K., Hirao K. Communication: A new hybrid exchange correlation functional for band-gap calculations using a short-range Gaussian attenuation (Gaussian–Perdue–Burke–Ernzerhof). *J. Chem. Phys.* 2011. **135**. P. 07110 (4 p.). https://doi.org/10.1063/1.3628522.
32. Senz St., Blum W., Hesse D. The effect of stress on cubic-to-tetragonal phase transitions in Mg_2TiO_4 and Mg_2GeO_4. *Phil. Mag. A.* 2001. **81**, No 1. P. 109–124. https://doi.org/10.1080/01418610108216621.
33. Wang C.P., Shieh S.R., Withers A.C. *et al.* Raman and X-ray diffraction study of pressure-induced phase transition in synthetic Mg_2TiO_4. *Sci Rep*. 2020. **10**. P. 6278. https://doi.org/10.1038/s41598-020-63202-5.
34. Pilania G., Kocevski V., Valdez J.A. *et al.* Prediction of structure and cation ordering in an ordered normal-inverse double spinel. *Commun. Mater.* 2020. **1**, No 1. P. 84 (11 p.). https://doi.org/10.1038/s43246-020-00082-2.
35. Huang C.S., Chang M.C., Huang C.L., Lin S.K. Thin-film photoluminescent properties and the atomistic model of Mg_2TiO_4 as a non-rare earth matrix material for red-emitting phosphor. *J. Electron. Mater.* 2016. **45**. P. 6214–6221. https://doi.org/10.1007/s11664-016-4846-1.

Authors and CV

Kashirina Nataliia I. PhD, Senior Researcher at the Department of Sensor Systems of the V. Lashkaryov Institute of Semiconductor Physics, NASU. Co-author of over 100 publications, 1 monograph, and 8 collective monographs. Field of research: physics of semiconductor materials and low-dimensional systems, modeling of localized and autolocalized states, and polaron effects in condensed matter. https://orcid.org/0000-0001-5863-4311.

Borkovska Lyudmyla V. Doctor of Sciences in Physics and Mathematics, Head of the Department of Sensor Systems, V. Lashkaryov Institute of Semiconductor Physics, NASU. Author of more than 95 articles, 2 patents, and co-author of 7 collective monographs. Field of research: optical sensors, solid-state luminescent materials, light-emitting devices and structures, and modification of physical properties of solids by interacting with laser radiation. https://orcid.org/0000-0002-7832-3796, e-mail: l_borkovska@ukr.net

Kashyrina Yaroslavna O., PhD in Physical Chemistry (Taras Shevchenko National University of Kyiv, 2024), Research Scientist at the Frantsevich Institute for Problems of Materials Science, NASU. Co-author of over 30 publications. Field of research: thermodynamic properties and structure of liquid and amorphous alloys, electron-phonon interaction in condensed matter; modern computer simulations of condensed matter. E-mail: yasya.loba@gmail.com, https://orcid.org/0000-0002-2901-6140

Muratov Oleksii S., PhD in Physical Chemistry, Researcher at the Chemistry Department of the Taras Shevchenko National University of Kyiv. He is the co-author of over 30 publications and 1 textbook. The area of his scientific interests includes structure of liquid alloys as well as modern computer simulations of condensed matter.
E-mail: muratov_os@univ.kiev.ua,
https://orcid.org/0000-0001-9416-3334

Roik Oleksandr S., Doctor of Sciences in Chemistry, Professor at the Chemistry Department of the Taras Shevchenko National University of Kyiv. Authored over 90 publications and 5 textbooks. Field of research: high-temperature X-ray diffraction studies of liquid alloys and molten salts, structure and physical properties of amorphous and nanocrystalline alloys, nanoporous metallic materials, electrochemistry as well as molecular dynamics and reverse Monte Carlo simulations of liquids and solids. E-mail: oleksandr_roik@knu.ua, https://orcid.org/0000-0001-9705-1100

Authors' contributions

Kashirina N.I.: conceptualization, methodology, investigation, software, writing – original draft preparation, writing review & editing.
Borkovska L.V.: validation, supervision, resources, writing review & editing, project administration.
Kashyrina Ya.O.: software, visualization, validation, writing – original draft, writing – review & editing.
Muratov O.S.: software, formal analysis, methodology, validation, visualization, writing – review & editing.
Roik O.S.: resources, software, supervision, writing – review & editing, project administration.

Розподіл атомів Mg та Ti за октаедричними позиціями та фізичні властивості Mg_2TiO_4

Н.І. Каширіна, Л.В. Борковська, Я.О. Каширіна, О.С. Муратов, О.С. Роїк

Анотація. Кераміка на основі Mg_2TiO_4 (MTO) широко використовується в численних сучасних квантових електронних пристроях. У роботі досліджено кубічні та тетрагональні модифікації MTO. Розраховано ширину забороненої зони та густину електронних станів кубічного MTO для різних розподілів атомів Mg та Ti за октаедричними позиціями в елементарній комірці. Розглянуто як випадкові розподіли атомів по октаедричних позиціях, так і високосиметричні комбінації. Побудовано залежність ширини забороненої зони від повної енергії елементарної комірки. Ширина забороненої зони збільшується зі зменшенням вільної енергії кристала. Показано, що високосиметричний розподіл атомів по октаедричних позиціях приводить до переходу кубічного MTO до тетрагональної сингонії з нижчою енергією порівняно з кубічним MTO з випадковим розподілом атомів по октаедричних позиціях. Ширина забороненої зони для кубічного MTO з випадковим розподілом атомів магнію та титану по октаедричних позиціях, розрахована за допомогою програмного пакету Vienna Ab initio Simulation Package (VASP), дорівнює 4,086 еВ. Отримані результати добре узгоджуються з експериментальними даними. Розрахована ширина забороненої зони для тетрагонального MTO дорівнює 4,988 еВ.

Ключові слова: Mg_2TiO_4, обернена шпінель, розрахунок зонної структури, густина станів.